HHS Public Access

Author manuscript

Dev Cell. Author manuscript; available in PMC 2020 May 20.

Published in final edited form as:

Dev Cell. 2019 May 20; 49(4): 632–642.e7. doi:10.1016/j.devcel.2019.04.032.

The long noncoding RNA *Pnky* is a *trans*-acting regulator of cortical development *in vivo*

Rebecca E. Andersen[1,2,3,†], **Sung Jun Hong**[1,2,3,†], **Justin J. Lim**[6], **Miao Cui**[1,2], **Brock A. Harpur**[6], **Elizabeth Hwang**[1,2,4], **Ryan N. Delgado**[1,2,4], **Alexander D. Ramos**[1,2,4], **Siyuan John Liu**[1,2,4], **Benjamin J. Blencowe**[6], and **Daniel A. Lim**[1,2,5,*]

[1]Department of Neurological Surgery, University of California, San Francisco, San Francisco, CA 94143, USA.

[2]Eli and Edythe Broad Center of Regeneration Medicine and Stem Cell Research, University of California, San Francisco, San Francisco, CA 94143, USA.

[3]Developmental and Stem Cell Biology Graduate Program, University of California, San Francisco, San Francisco, CA 94143, USA.

[4]Medical Scientist Training Program, Biomedical Sciences Graduate Program, University of California, San Francisco, San Francisco, CA 94143, USA.

[5]San Francisco Veterans Affairs Medical Center, San Francisco, CA 94121, USA.

[6]Donnelly Centre and Department of Molecular Genetics, University of Toronto, 160 College Street, Toronto, ON M5S 3E1, Canada.

SUMMARY

While it is now appreciated that certain long noncoding RNAs (lncRNAs) have important functions in cell biology, relatively few have been shown to regulate development *in vivo*, particularly with genetic strategies that establish *cis* versus *trans* mechanisms. *Pnky* is a nuclear-enriched lncRNA that is transcribed divergently from the neighboring proneural transcription factor *Pou3f2*. Here we show that conditional deletion of *Pnky* from the developing cortex regulates the production of projection neurons from neural stem cells (NSCs) in a cell-autonomous manner, altering postnatal cortical lamination. Surprisingly, *Pou3f2* expression is not disrupted by deletion of the entire *Pnky* gene. Moreover, expression of *Pnky* from a BAC transgene rescues the differential gene expression and increased neurogenesis of *Pnky*-knockout NSCs, as well as the

*Corresponding author, lead contact: Daniel.Lim@ucsf.edu.
†Equal contribution.

AUTHOR CONTRIBUTIONS

R.E.A. designed, performed, and analyzed experiments, compiled figures, and wrote the manuscript. SJ.H. designed, performed, and analyzed experiments. J.J.L. and B.A.H. performed alternative splicing analysis. M.C. performed RIP experiments. E.H. and R.N.D. performed differential expression analysis. A.D.R. contributed to the design and generation of mouse lines. S.J.L. generated the Circos plot. B.J.B. supervised alternative splicing analysis. D.A.L. supervised experiments and wrote the manuscript.

DECLARATION OF INTERESTS

The authors declare no competing interests.

developmental phenotypes of *Pnky*-deletion *in vivo*. Thus, despite being transcribed divergently from a key developmental transcription factor, the lncRNA *Pnky* regulates development in *trans*.

eTOC:

Long noncoding RNAs (lncRNAs) can play important roles in cells, but the *in vivo* functions of most lncRNAs remain unclear. Andersen, Hong et al. find that the lncRNA *Pnky* regulates neuron production in the developing mouse cortex in a cell-autonomous manner and further demonstrate that *Pnky* functions in trans.

INTRODUCTION

The mammalian genome produces tens of thousands of distinct long noncoding RNAs (lncRNAs) – transcripts longer than 200 nucleotides (nt) that do not encode proteins (Djebali et al., 2012) – and a growing number of lncRNAs have been shown to play important biological roles in cultured cells. However, because genetic studies of lncRNA function *in vivo* are currently lacking, the biological significance of most lncRNAs for the development of tissues and organs *in vivo* is unclear (Nakagawa, 2016). Moreover, for most lncRNAs that have been discovered to have function, the mechanism(s) by which they regulate cell biology remain enigmatic (Bassett et al., 2014; Kopp and Mendell, 2018). A fundamentally important question is whether the lncRNA locus functions in *cis* – regulating local gene transcription on the same chromosome – and/or in *trans* – producing a molecule that functions at cellular locations distant from where it is produced.

Pnky is an 825 nt, evolutionarily-conserved, nuclear-enriched, polyadenylated lncRNA that is expressed in neural stem cells (NSCs) both *in vitro* and *in vivo* (Ramos et al., 2015). We have previously shown that short-hairpin RNA (shRNA)-mediated *Pnky* knockdown (KD) increases neuronal production from NSCs in culture as well as in the developing cortex (Ramos et al., 2015). However, methods that directly target lncRNA transcripts for degradation, such as the use of shRNAs and antisense oligonucleotides (ASOs), do not clearly distinguish between *cis*- and *trans*-acting mechanisms, particularly for lncRNAs that localize to the nucleus (Kopp and Mendell, 2018; Wagschal et al., 2012). In addition to reducing potential *trans*-activities of a lncRNA, KD of the lncRNA can also modulate local gene expression (Luo et al., 2016; Ørom et al., 2010; Wang et al., 2011). Finally, in addition to potential off-target effects and issues related to partial KD, the use of shRNAs and ASOs for *in vivo* developmental studies can be technically challenging (Kaczmarek et al., 2017).

For a relatively small number of lncRNAs, genetic deletions have been used to reveal developmental phenotypes *in vivo* (Bassett et al., 2014). However, in addition to testing potential *trans* function, genetic deletions can also perturb *cis*-regulatory mechanisms (*e.g.*, through the removal of transcriptional enhancers). The insertion of poly-adenylation (poly-A) signals into lncRNAs can disrupt transcriptional elongation and reveal *in vivo* phenotypes (Anderson et al., 2016; Bond et al., 2009), but given that transcriptional activity local to the lncRNA transcriptional start site (TSS) can often regulate nearby genes, poly-A insertion may not inactivate all potential lncRNA functions. Despite these and other known shortcomings, genetic methods are powerful tools for studying phenotypes *in vivo* and

understanding molecular mechanism, particularly when different genetic strategies are combined in a complementary manner.

Here, we integrated multiple genetic approaches to investigate the function and molecular mechanism of the lncRNA *Pnky* in brain development. The TSS of *Pnky* is located ~2.2kb from that of the neighboring gene *Pou3f2* (Dominguez et al., 2013), which is transcribed in the opposite direction. This "divergent" orientation has been described for approximately 20% of mammalian lncRNAs and has been found to predict a *cis* regulatory interaction with the coding gene neighbor (Luo et al., 2016). Surprisingly, *Pnky*-deletion did not disrupt the expression of *Pou3f2*. To test the alternative hypothesis – that *Pnky* regulates neural development in *trans* – we generated transgenic mice that express *Pnky* at physiological levels from an integrated bacterial artificial chromosome (BAC) construct. *Pnky* expressed from this BAC rescued the differential gene expression and cellular phenotype of *Pnky*-knockout NSCs, as well as the developmental phenotypes of *Pnky*-deletion *in vivo*. Thus, the integration of these complementary genetic strategies reveals that *Pnky* functions in *trans* to regulate brain development *in vivo*.

RESULTS

Generation of a conditional *Pnky* deletion allele

To enable temporal and cell type-specific control over *Pnky* loss-of-function *in vivo*, we used a Cre-loxP strategy. In the design of this genetic approach, we remained agnostic about the specific mechanism(s) by which *Pnky* might function. We therefore generated a conditional *Pnky* allele that removes the broad range of potential lncRNA mechanisms (both *cis* and *trans*) by flanking the entire *Pnky* gene including its TSS with loxP sites (Fig. 1A-B), and we produced mice with this "floxed" *Pnky* allele ($Pnky^{F}$).

The genetic removal of an entire lncRNA locus might not produce the same phenotype as degradation of the lncRNA transcript itself (Bassett et al., 2014; Nakagawa, 2016). In NSC cultures from the postnatal mouse ventricular-subventricular zone (V-SVZ), shRNA-mediated *Pnky* KD increases neurogenesis by 3-4 fold (Ramos et al., 2015). We therefore investigated whether acute *Pnky* conditional knockout (*Pnky*-cKO) in V-SVZ NSC cultures would also increase neurogenesis. V-SVZ NSC cultures were established from postnatal $Pnky^{F/F}$ or wild-type ($Pnky^{+/+}$) mice that carried the tamoxifen-inducible UBC-Cre-ERT2 transgene. To induce Cre-mediated recombination, cultures were treated with 4-hydroxytamoxifen (4-OHT) (Fig. S1A). In $Pnky^{F/F}$;UBC-Cre-ERT2 cultures, 4-OHT treatment abolished *Pnky* expression (−95.6%) (Fig. 1C), and these *Pnky*-cKO NSCs exhibited increased neurogenesis, producing nearly 6-fold more neurons than control cultures (Fig. 1D-E). Thus, conditional deletion of the entire *Pnky* gene produces a phenotype similar to that of *Pnky* transcript KD in cultured NSCs.

Divergent lncRNAs are transcribed in the opposite direction of nearby genes in a "head-to-head" configuration (Luo et al., 2016), and *Pnky* is divergent to the proneural transcription factor *Pou3f2* (Dominguez et al., 2013). In a study of 12 different lncRNAs divergent to transcription factors, shRNA-mediated lncRNA KD consistently downregulates the coding gene neighbor (Luo et al., 2016). We re-analyzed RNA-sequencing (RNA-seq) data of

shRNA-mediated *Pnky* KD in V-SVZ NSCs (Ramos et al., 2015) and did not observe differential expression of *Pou3f2* or any other gene +/− 2.5 MB from *Pnky* (Fig. S1B). However, it is unclear whether shRNA-mediated KD affects the processes of transcription and splicing of RNA transcripts (Wagschal et al., 2012; West et al., 2004). This mechanistic consideration is important as some lncRNAs – independent of the specific transcripts themselves – regulate their divergent gene neighbor through these processes (Engreitz et al., 2016). Surprisingly, *Pnky*-cKO did not affect the abundance of *Pou3f2* transcript in V-SVZ NSCs ($p = 0.40$) (Fig. 1C). Thus, *Pou3f2* expression in cultured NSCs does not appear to require the *Pnky* transcript, processes related to its local transcription, splicing of the lncRNA, or potential regulatory elements contained within the deleted DNA sequence.

Pnky regulates development of the mouse neocortex

The mammalian neocortex is a dorsal brain structure comprised of six layers of projection neurons, and the proper development of these layers is critical to cognitive function (Lodato and Arlotta, 2015; Molyneaux et al., 2007; Rubenstein, 2011). In addition to projection neurons, the cortex contains many interneurons that are dispersed throughout. In the embryonic brain, cortical projection neurons are born locally from NSCs in the dorsal brain (pallium), whereas cortical interneurons arise from ventral regions (subpallium). During development, changes in the production of cortical interneurons can modulate the genesis of projection neurons (Silva et al., 2018), and vice versa (Lodato et al., 2011). *Pnky* is expressed in NSCs in both the pallium and subpallium of the embryonic brain (Ramos et al., 2015). Thus, to investigate whether *Pnky* directly regulates the production of cortical projection neurons, we focused our *in vivo* analysis on the cell lineages derived from pallial NSCs.

We targeted *Pnky*-cKO to pallial NSCs with $Emx1^{Cre}$, which expresses Cre in the pallium beginning at ~ embryonic day (E) 9.5 (Briata et al., 1996; Gorski et al., 2002; Simeone et al., 1992) (Fig. S1C). Embryonic brain NSCs reside in the ventricular zone (VZ), and *in situ* hybridization (ISH) revealed *Pnky* expression in the pallial VZ by E10.0 (Fig. S1D). In $Pnky^{F/F};Emx1^{Cre}$ mice, *Pnky* expression in the pallium was ablated as assessed by ISH, with very few *Pnky* transcripts detected in the pallium at E10.0 (Fig. S1D), and none by E13.5 (Fig. 1F) or postnatal day (P) 14 (Fig. S1E). As expected, in the subpallium of $Pnky^{F/F};Emx1^{Cre}$ mice, *Pnky* expression was not decreased (Fig. 1F, S1D). Thus, before the onset of cortical neurogenesis, $Pnky^{F/F};Emx1^{Cre}$ mice have undergone *Pnky*-cKO selectively in the NSCs that give rise to cortical projection neurons.

Despite evidence of homozygous *Pnky* deletion, the expression of POU3F2 in the $Pnky^{F/F};Emx1^{Cre}$ pallium was indistinguishable from that of littermate controls (Fig. 1G, S1F). Consistent with these immunohistochemical (IHC) results, RNA-seq analysis of acutely-dissected E12.5 pallium showed that *Pnky*-cKO abolished *Pnky* expression (Fig. S1G) without perturbing *Pou3f2* transcript levels (adjusted $p = 0.37$) (Fig. S1H). While *Pnky*-cKO resulted in differential expression of genes with roles in cortical development and neurogenesis, including *Lhx9* (Peukert et al., 2011) and *Fezf2* (Molyneaux et al., 2005; Zhang et al., 2014), differential expression was not observed within +/− 20 MB of *Pnky* (Table S1). Moreover, we did not find POU3F2 binding motifs within the promoter region of

any of the differentially-expressed genes (Table S1). The E12.5 cortex of *Pnky*$^{F/F}$;*Emx1*^{Cre} mice also exhibited changes in alternative splicing (Fig. S1I, Table S1), affecting transcripts with known neurodevelopmental roles such as *Ank3* (Durak et al., 2015) and *Tcf12* (Mesman and Smidt, 2017). Thus, in the early embryonic pallium, *Pnky*-cKO affects the abundance and splicing of transcripts related to neural development, but does not disrupt the expression of *Pou3f2* mRNA or protein.

The development of the laminar structure of the cortex progresses temporally in an "inside-out" manner: NSCs first give rise to projection neurons for the deep layers (5 and 6), while later-born neurons migrate past them to form the upper layers (2/3 and 4) (Lodato and Arlotta, 2015). In mice, the birth of deep layer neurons peaks around E13.5. As compared to littermate controls, the *Pnky*$^{F/F}$;*Emx1*^{Cre} cortex of E13.5 mice had increased numbers of CTIP2+ neurons in the cortical plate (CP) (+24.3%) (Fig. 2A-B). This increase in neurogenesis was accompanied by a decrease in proliferating VZ cells as determined by analysis of phosphorylated histone H3 (pH3) (−17.3%) (Fig. 2C-D) and phosphorylated Vimentin (pVIM) (−11.8%) (Fig. S2A-B). Thus, consistent with prior results obtained with shRNA-mediated *Pnky* KD (Ramos et al., 2015), *Pnky*-cKO targeted to pallial NSCs increases neuronal production but decreases the pool of proliferative NSCs.

Given the increase in early-born CTIP2+ neurons at E13.5 (Fig. 2A-B), we assessed for changes in the number of deep layer neurons at P14, when the laminar structure of the cortex is fully evident. As compared to littermate controls, *Pnky*$^{F/F}$;*Emx1*^{Cre} mice exhibited an increased number of CTIP2+ neurons in layer 6, the deepest cortical layer (+8.1%) (Fig. 2E-F). Since the number of proliferative VZ cells was reduced in *Pnky*$^{F/F}$;*Emx1*^{Cre} mice at E13.5 (Fig. 2C-D, S2A-B), and the peak of upper layer neurogenesis occurs later (~E15.5), we considered that upper layer neurogenesis might be affected in *Pnky*$^{F/F}$;*Emx1*^{Cre} mice. As compared to littermate controls, the P14 cortex of *Pnky*$^{F/F}$;*Emx1*^{Cre} mice exhibited fewer CUX1+ neurons in the upper cortical layers (−14.4%) (Fig. 2G-H). Furthermore, we used 5-bromo-2'-deoxyuridine (BrdU) to label neurons born at E15.5, and the P14 cortex of *Pnky*$^{F/F}$;*Emx1*^{Cre} mice also had reduced numbers of BrdU+;CUX1+ cells in the upper layers (−14.5%) (Fig. S2C). Essentially all BrdU+ cells in all mice were located in the upper layers, and there was no change in the proportion these cells that were also CUX1+ ($p = 0.25$) (Fig. S2D), indicating that *Pnky*-deletion does not simply cause a loss of CUX1 expression or mis-specification. Thus, *Pnky*-cKO in the early embryonic pallium causes malformation of the postnatal neocortex, increasing the number of deep layer neurons while decreasing the population of upper layer neurons.

To determine whether *Pnky* function is cell-autonomous, we targeted *Pnky*-cKO to a small cohort of NSCs by injecting a Cre-expressing adenovirus (Ad:Cre) (Fig. S3A-B) into the lateral ventricles of E13.5 *Pnky*$^{F/F}$ mice or wild-type (*Pnky*$^{+/+}$) littermate controls *in utero* (Fig. 3A, S3C). For fate-tracing analysis, these mice carried the Ai14 transgenic reporter that expresses tdTomato after Cre-mediated recombination (Fig. 3B). Two days after Ad:Cre injection, *Pnky*$^{F/F}$;Ai14 mice exhibited an increase in the proportion of tdTomato+ cells that were found in the CP (+82.7%) (Fig. 3C, D), as well as in the proportion of CTIP2+ CP cells (+86.4%) (Fig. 3E). To investigate whether this increase in early neurogenesis leads to changes in the postnatal cortex, we analyzed mice 20 days post-injection (at P14).

Consistent with *Pnky*-cKO at E13.5 causing an overproduction of deep layer neurons at the expense of the later upper layer neurons, the postnatal cortex of $Pnky^{F/F}$;Ai14 mice exhibited an increase in the ratio of CTIP2+ deep layer to CUX1+ upper layer cells within the tdTomato+ population (+19.9%) (Fig. 3F-G, S3D). These results indicate that *Pnky* regulates cortical neurogenesis in a cell-autonomous manner.

Pnky functions in *trans* to regulate cortical development

Given the lack of evidence for *Pnky* regulating *Pou3f2* or other genes in *cis*, we developed genetic methods to test whether *Pnky* functions in *trans*. We obtained a bacterial artificial chromosome (BAC) containing ~170kb of the genomic sequence surrounding *Pnky* and removed the coding sequence of *Pou3f2*, the only other complete gene in this BAC (Fig. 4A, S4A). We then generated transgenic mice (BAC^{Pnky}) that express *Pnky* from this modified BAC construct and bred them with mice carrying the $Pnky^{F}$ allele. We established cortical NSC (cNSC) cultures from $Pnky^{+/+}$, $Pnky^{F/F}$, and $Pnky^{F/F}$;BAC^{Pnky} E12.5 embryos, and used Ad:Cre to induce recombination. Three days later, we performed RNA-seq from these cultures as well as paired untreated control cultures (Fig. S4B). While the addition of Ad:Cre to $Pnk^{F/F}$ cultures abolished the expression of *Pnky*, the presence of BAC^{Pnky} maintained *Pnky* at approximately 20% of wildtype levels (Fig. 4B).

In these undifferentiated cNSCs, *Pnky*-cKO resulted in the differential expression of 55 other genes (Fig. 4C, Table S2), including genes known to have roles in neurodevelopment such as *Miat (Gomafu)* (Aprea et al., 2013; Barry et al., 2014; Spadaro et al., 2015) and *Erbb4* (Perez-Garcia, 2015). None of the differentially-expressed genes contained POU3F2 binding motifs within their promoter regions (Table S2). Strikingly, the vast majority (47 of 55, 85.5%) of the genes that were differentially expressed with *Pnky*-cKO was significantly rescued by the presence of BAC^{Pnky}, such that these genes were no longer differentially expressed in $Pnky^{F/F}$;BAC^{Pnky} cultures (Fig. 4D). Of the 27 genes that were increased in *Pnky*-cKO cultures, 21 (77.8%) were decreased by the presence of BAC^{Pnky}. Similarly, 92.9% (26 of 28) of the genes downregulated by *Pnky*-cKO were increased by BAC^{Pnky}. Of note, the transcriptional changes related to BAC^{Pnky} were significantly restricted to those genes differentially expressed in *Pnky*-cKO cells ($p = 1.33\times10^{-51}$, hypergeometric test). Thus, expression of *Pnky* from a BAC transgene specifically rescues the transcriptional changes that result from deletion of endogenous *Pnky*.

In postnatal V-SVZ NSCs, *Pnky* physically interacts with PTBP1 (Ramos et al., 2015) – an mRNA splicing factor that regulates neurogenesis in NSCs (Zhang et al., 2016). RNA immunoprecipitation (RIP) with PTBP1 antibodies also enriched the *Pnky* transcript from cNSC cultures (Fig. 4E). In cNSCs, *Pnky*-cKO affected 220 splicing events as compared to $Pnky^{+/+}$ controls (Fig. 4F, Table S2), and 22 of these events were rescued (no longer significantly differentially spliced) by the presence of BAC^{Pnky} ($p = 1.99\times10^{-8}$, hypergeometric test) (Fig. 4G). We also compared the splicing changes that occur upon loss of *Pnky* with two previously-generated datasets of PTBP1 KD in different neural cells (Raj et al., 2014; Ramos et al., 2015). Interestingly, 47 events were also differentially spliced upon PTBP1 KD in at least one dataset, and 13 of these were differentially spliced in both PTBP1 datasets ($X^2=7.7$; $p = 0.0006$) (Fig. S4C). These data suggest that in addition to

regulating the abundance of specific transcripts (Fig. 4C-D), *Pnky* also influences mRNA splicing.

After removal of mitogenic growth factors, cNSCs produce neurons in culture (Fig. S4B). Coherent with the increase in cortical neurogenesis observed with *Pnky*-cKO *in vivo* and the analysis of V-SVZ NSCs *in vitro*, cNSCs with *Pnky*-cKO produced ~3-fold more neurons as compared to the $Pnky^{+/+}$ controls (+2.88 fold) (Fig. 4H-I). The presence of BAC^{Pnky} in *Pnky*-cKO cNSCs reduced neurogenesis to levels observed in $Pnky^{+/+}$ cultures ($p = 0.41$) (Fig. 4H-I), indicating that the BAC^{Pnky} transgene can rescue the neurogenic phenotype of *Pnky*-cKO *in vitro*.

To investigate whether BAC^{Pnky} can rescue the phenotype of *Pnky*-deletion *in vivo*, we generated mice with germline *Pnky*-deletion ($Pnky^{null/nul}$) and crossed these two mouse lines to produce $Pnky^{null/null}$;BAC^{Pnky} mice (Fig. S4D). While $Pnky^{null/null}$ mice had no detectable *Pnky* transcripts, $Pnky^{null/null}$;BAC^{Pnky} mice exhibited a similar pattern and level of *Pnky* expression as $Pnky^{+/+}$ animals (Fig. 4J, S4E). Therefore, expression of *Pnky* from the BAC mimics that from the endogenous *Pnky* locus. In comparison to $Pnky^{+/+}$ littermates, E13.5 $Pnky^{null/null}$ embryos had fewer CTIP2+ neurons in the CP (−16.6%) (Fig. 4K-L). This decrease in neurogenesis may relate to the constitutive absence of *Pnky* causing an earlier loss of proliferative NSCs. Consistent with this notion, we observed a decrease in proliferative pH3+ progenitor cells in the VZ of $Pnky^{null/null}$ mice (−9.7%) (Fig. 4M-N), and the overall thickness of the cortex was also reduced in these animals (Fig S4F). Importantly, the presence of the BAC^{Pnky} transgene was sufficient to rescue all of these phenotypes in $Pnky^{null/null}$;BAC^{Pnky} mice (Fig. 4K-N,S4F). Thus,the expression of *Pnky* in *trans* from a BAC rescues the phenotype of *Pnky*-deletion in the developing cortex *in vivo*.

DISCUSSION

There are currently few genetic studies of lncRNA function *in vivo*, and thus the biological significance of most lncRNAs during mammalian development is unclear (Bassett et al., 2014; Nakagawa, 2016). Using a combination of genetic methods in mice to systematically study the function and genetic mechanism of *Pnky*, we show that this lncRNA functions in *trans* to regulate the development of the neocortex. By targeting conditional *Pnky* deletion to specific cell types in the embryonic brain, we found that *Pnky* regulates the genesis of neocortical projection neurons in a cell-autonomous manner. Surprisingly, *Pnky*-deletion did not produce evidence that this lncRNA regulates gene expression in *cis*. Moreover, when expressed from a BAC transgene, *Pnky* rescued both the differential gene expression and cellular phenotype of cultured *Pnky*-cKO NSCs. BAC^{Pnky} was also sufficient to rescue the *in vivo* phenotypes of *Pnky*-deletion in the developing cortex, indicating that *Pnky* functions in *trans*.

The production of projection neurons for the different layers of the mammalian neocortex is a critical, highly regulated aspect of brain development (Lodato and Arlotta, 2015). For instance, deletion of the transcription factor *Eomes/Tbr2* in the embryonic brain decreases the CUX1+ upper layers by ~20% (Arnold et al., 2008). *Pnky*-cKO targeted to NSCs in the early embryonic pallium with $Emx1^{Cre}$ altered postnatal cortical lamination such that there

were ~10% more deep layer 6 neurons and ~15% fewer upper layer neurons. This postnatal phenotype corresponded to an increase in early neurogenesis (during deep layer production) *in vivo* at the expense of proliferating VZ cells, which later give rise to upper layer neurons. Coherent with these *in vivo* observations, acute *Pnky*-cKO in cultured NSCs also increased neurogenesis. This *in vitro* phenotype was previously observed with shRNA-mediated *Pnky* KD, indicating that deletion of the *Pnky* gene has similar effects to targeting the transcript. The cellular phenotypes of *Pnky*-cKO and *Pnky* KD were more dramatic in cultured NSCs as compared to those in the developing cortex, suggesting that there are mechanisms *in vivo* that can partially compensate for the loss of *Pnky* transcript.

Interestingly, constitutive deletion of the lncRNA locus for *linc-Brn1b* also results in more (~20%) deep layer neurons and fewer (~10%) upper layer cells in the postnatal cortex (Sauvageau et al., 2013). However, in contrast to *Pnky*-KO, deletion of *linc-Brn1b* reduces expression of its neighboring transcription factor, *Pou3f3* (Sauvageau et al., 2013), which is a paralog of the *Pnky* neighbor *Pou3f2*. Another lncRNA, *linc-Brn1a* (a.k.a. *Pou3f3os*) is divergent to *Pou3f3* and shRNA-mediated KD of this lncRNA also reduces levels of *Pou3f3* (Luo et al., 2016). Thus, even closely related genes such as *Pou3f2* and *Pou3f3* appear to have very different functional relationships with nearby lncRNAs.

Divergent lncRNAs are strongly predicted to regulate the expression of transcription factor gene neighbors (Luo et al., 2016). Even the processes of lncRNA transcription and splicing, independent of the mature lncRNA transcript itself, can regulate expression of the divergent gene neighbor (Engreitz et al., 2016; Kopp and Mendell, 2018). For example, the lncRNA upperhand (*Uph*) is divergent to the transcription factor *Hand2*, and insertion of a poly-A cassette into *Uph* abolishes the expression of *Hand2* in *cis*, resulting in severe cardiac defects *in vivo* (Anderson et al., 2016). However, ASO-mediated KD of *Uph* does not affect *Hand2* levels. Importantly, *Uph* is transcribed through known enhancers of *Hand2*, and transcription of this lncRNA appears to establish a more permissive chromatin state for these enhancers. In contrast, *Pnky*-deletion did not affect expression of *Pou3f2*. Of note, the *Pnky* locus is not known to harbor transcriptional enhancers, and we have not observed strong enhancer-like activity of *Pnky* DNA sequences in cell culture reporter assays (unpublished observations). We therefore speculate that whether a divergent, functional lncRNA has *cis* and/or *trans* mechanisms relates in part to the local presence (or absence) of transcriptional enhancers.

Divergent lncRNAs can also regulate the function of the protein that arises from the coding gene neighbor. For instance, the lncRNA *Paupar* – which is transcribed through an enhancer of its neighbor *Pax6* – not only regulates *Pax6* expression but also physically interacts with the PAX6 transcription factor to affect its regulation of target genes (Pavlaki et al., 2018; Vance et al., 2014). In the developing retina, the divergent lncRNA *Six3OS* appears to act as a molecular scaffold, regulating the activity of its transcription factor neighbor, SIX3 (Rapicavoli et al., 2011). While modulation of POU3F2 activity is a plausible mechanism of *Pnky* function, we have not observed interactions between *Pnky* transcript and POU3F2 protein (not shown), and *Pnky*-deletion did not affect the expression of potential POU3F2 target genes.

It remains possible that *Pnky* regulates *Pou3f2* in other cellular contexts, or alters transcriptional dynamics that might not change steady-state levels of mRNA (Imayoshi and Kageyama, 2014; Lenstra et al., 2016). Importantly, lncRNA mechanisms are not necessarily mutually exclusive, and there are examples of lncRNAs that carry out multiple distinct molecular roles through both *cis* and *trans* mechanisms (Cajigas et al., 2018; Pavlaki et al., 2018; Vance et al., 2014). However, the rescue of *Pnky*-deletion phenotypes by BAC^{Pnky} strongly suggests that *Pnky* primarily functions in *trans* in NSCs. While BAC^{Pnky} also contains the untranslated regions (UTRs) of *Pou3f2*, and it is conceivable that these sequences contribute to the rescue, it is remarkable that essentially all of the differential gene expression resulting from *Pnky*-deletion was significantly and specifically rescued by BAC^{Pnky}. *Pnky* RNA physically interacts with PTBP1, a factor that regulates both transcript abundance and splicing, and BAC^{Pnky} rescued ~10% of the differentially-spliced events in *Pnky*-cKO NSCs. While there was significant overlap between the differentially-spliced events upon *Pnky*-cKO and *Ptbp1*-KD, how *Pnky* might affect PTBP1-dependent splicing remains to be discovered. Furthermore, *Pnky* may have additional roles that are independent of PTBP1. Future work to more comprehensively identify proteins that interact with *Pnky* will be important to further determine the mechanism(s) by which this lncRNA regulates transcript abundance and splicing, and ultimately neural development.

The developing brain expresses many thousands of different lncRNAs, and there are emerging examples of lncRNAs with relevance to neurodevelopmental disorders (Briggs et al., 2015; Meng et al., 2015), underscoring the need to determine the functions of lncRNAs during brain development in animal models. While efforts have been made to predict lncRNA biology from their underlying DNA sequence and genomic location (Engreitz et al., 2016; Liu et al., 2017; Luo et al., 2016), at this point in this emerging field of research, testing individual lncRNAs systematically will likely be required to decipher fundamental aspects of their developmental function and mechanism. Because the range of potential mechanisms of lncRNAs is fundamentally more broad (*cis* and *trans*) than protein coding genes or microRNAs, it is unlikely that any one experimental method will be sufficient to lay the groundwork for understanding molecular mechanism, and instead an integration of multiple approaches will often be required (Liu and Lim, 2018). Moving forward, *in vivo* studies of lncRNA function will serve as a crucial foundation for understanding how this class of noncoding transcripts can regulate normal brain development and contribute to neurological disorders.

STAR METHODS

CONTACT FOR REAGENT AND RESOURCE SHARING

Further information and requests for resources and reagents should be directed to and will be fulfilled by the Lead Contact, Dr. Daniel Lim (Daniel.Lim@ucsf.edu).

EXPERIMENTAL MODEL AND SUBJECT DETAILS

Mus musculus—All mice were group-housed and maintained in the University of California, San Francisco Laboratory Animal Resource Center under protocols approved by the Institutional Animal Care and Use Committee. All relevant ethical regulations were

followed. Mice of both sexes were used for all experiments, and were analyzed at multiple ages between E10.0 and P14 as described in the text and figure legends for each experiment. All samples were analyzed relative to littermates. For *Emx1*^{Cre} experiments, control samples were *Pnky*$^{+/+}$;*Emx1*^{Cre} or any combination of *Pnky* alleles in the absence of *Emx1*^{Cre}. Details regarding mouse strains are as follows (see also Key Resources Table):

UBC-Cre-ERT2: Tg(UBC-cre/ERT2)1Ejb, described in (Ruzankina et al., 2007).

Emx1^{Cre}: *Emx1*$^{tm1(cre)Krj}$, described in (Gorski et al., 2002).

Ai14: Gt(ROSA)26Sor$^{tm14(CAG-tdTomato)Hze}$, described in (Madisen et al., 2010).

E2a-Cre: Tg(EIIa-cre)C5379Lmgd, described in (Lakso et al., 1996).

Primary cell culture: All cells were grown in humidified incubators at 37°C in 5% CO_2.

V-SVZ cultures: The brains of P7 mice were dissected out of the skull, and then a coronal slab of approximately 0.5 mm in thickness was obtained manually or by using a vibratome. Dissections were performed in ice-cold L15 medium (ThermoFisher 11415064) to collect the V-SVZ region along the lateral walls of the lateral ventricles. The tissue was dissociated with 300 μL of 0.25% trypsin-EDTA (ThermoFisher 25200056) with occasional agitation for 20 min at 37°C, and then the trypsin was quenched with 600 μL of N5 growth medium (see below). Cells were mechanically dissociated by trituration and then pelleted by centrifugation at 300 g for 5 min. Cells were resuspended in fresh N5 growth medium and plated in one well of a 12-well tissue culture plate per mouse.

Cells were grown in N5 growth medium: DMEM/F-12 with GlutaMAX (ThermoFisher 10565018) supplemented with 5% Fetal Bovine Serum (Fisher Scientific SH30070.03), N2 supplement (ThermoFisher 17502048, 1:100), 35 μg/mL bovine pituitary extract (ThermoFisher 13028014), Antibiotic-Antimycotic (ThermoFisher 15240062, 1:100), 20 ng/mL epidermal growth factor (EGF, PeproTech AF-100-15), and 20 ng/mL basic fibroblast growth factor (bFGF, PeproTech 100-18B).

For routine passaging, cells were grown to hyperconfluency and then dissociated using 0.25% trypsin-EDTA (ThermoFisher 25200056) for 3-5 minutes in the incubator. This was diluted with an equal volume of growth medium, and the cells were dissociated by trituration. Cells were pelleted as described above, then resuspended in fresh culture medium to plate in 2 times the original culture area.

For recombination using the tamoxifen-inducible UBC-Cre-ERT2 transgene, cultures were treated with 10nM 4-hydroxytamoxifen (4-OHT) for 48 hours. 4-OHT was reconstituted in EtOH, and all experimental cultures were normalized to paired EtOH-treated control cultures.

To differentiate the cells, cultures were grown to hyperconfluency and then the medium was replaced without EGF or FGF.

Cortical neural stem cell cultures: Tissue culture plates were prepared by coating with 1 mg/mL poly-D-lysine (Millipore A-003-E) for at least 4 hours in the incubator. This was rinsed twice with PBS or water and replaced with 5 μg/mL laminin (ThermoFisher 23017015) in the incubator O/N. As laminin is highly sensitive to drying, this was removed well-by-well and immediately replaced with enough culture medium to cover the surface of the well. Cells were then plated in the remaining volume.

Cultures of cNSCs were derived from E12.5 mice as described in (Currle et al., 2007), with modifications. The developing cortex was dissected from E12.5 embryos in ice-cold high-glucose DMEM (ThermoFisher 31053028) and then dissociated with 100 mL of 0.05% trypsin-EDTA (ThermoFisher 25300054) for 20 min at 37°C. Trypsinization was halted using 200 μL of 0.25 mg/mL soybean trypsin inhibitor (ThermoFisher 17075029). Cells were mechanically dissociated by trituration and then pelleted by centrifugation at 1000 g for 3 min. Cells were resuspended in 1mL of PBS to rinse, and then re-pelleted. Cells were finally resuspended in growth medium (see below) and plated in one well of a pre-treated (see above) 12-well tissue culture plate per embryo.

Cells were grown in the following medium slightly modified from (Hudlebusch et al., 2011): 50% DMEM/F-12 medium (ThermoFisher 11330057) and 50% Neurobasal medium (ThermoFisher 21103049) supplemented with N2 (ThermoFisher 17502048, 1:100), B27 (ThermoFisher 17504044, 1:50), Antibiotic-Antimycotic (ThermoFisher 15240062, 1:100), HEPES (ThermoFisher 15630080, 1:200), 2 μg/ml Heparin sodium salt (Millipore Sigma H3149), Bovine Albumin Fraction V (ThermoFisher 15260037, 1:750), MEM non-essential amino acids (ThermoFisher 11140050, 1:100), GlutaMAX (ThermoFisher 35050061, 1:100), Sodium Pyruvate (ThermoFisher 11360070, 1:100), β-mercaptoethanol (Millipore ES-007-E, 1:5000), 10 ng/ml epidermal growth factor (EGF, PeproTech AF-100-15) and 20 ng/ml basic fibroblast growth factor (bFGF, PeproTech 100-18B).

For routine passaging, cells were grown to confluency and then dissociated using StemPro Accutase (ThermoFisher A1110501) for 5 minutes in the incubator. This was diluted with an equal volume of growth medium, and the cells were dissociated by trituration. Cells were pelleted as described above, then resuspended in fresh culture medium to plate in 3 times the original culture area.

To differentiate the cells, cultures were grown to confluency and then the medium was replaced without EGF or FGF.

METHOD DETAILS

Generation of the *Pnky* conditional (*Pnky*^{F}) mouse line—A conditional allele of *Pnky* was created by inGenious Targeting Laboratory through homologous recombination in C57BL/6 × 129/SvEv hybrid embryonic stem (ES) cells. The targeting construct contained a Neomycin resistance cassette to enable drug selection of recombined cells. Targeted ES cells were microinjected into C57BL/6 blastocysts. Resulting chimeras with a high percentage agouti coat color were mated to C57BL/6 FLP mice to remove the Neomycin resistance cassette. The resulting *Pnky*^{F} allele has the entire *Pnky* gene flanked by loxP sites, with one

loxP site 727 bp upstream of the TSS and the other 938 bp downstream of the transcriptional end site (TES).

Generation of the *Pnky* constitutive deletion (*Pnky*^{null}) mouse line—Constitutive deletion of *Pnky* was obtained through mating the *Pnky*^{F} line to the germline-expressed E2a-Cre mouse line. Progeny with germline deletion of *Pnky* were then mated to wild-type mice to obtain *Pnky*$^{null/+}$ founders that lacked the E2a-Cre transgene.

Generation of the BAC*Pnky* mouse line—BAC clone RP23-451I6 was obtained from the BACPAC Resources Center and modified as shown (Fig. S4A) to remove the coding sequence (CDS) from *Pou3f2*, leaving the UTRs intact. Modifications were made as described in (Warming et al., 2005), and using the detailed protocols found at https://ncifrederick.cancer.gov/research/brb/protocol.aspx. We primarily used “Recombineering Protocol #3” and referred to “Recombineering Protocol #1” for additional details. The modified BAC was microinjected into C57BL/6 zygotes by the Transgenic Gene Targeting Core (Gladstone Institutes, UCSF).

Polymerase chain reaction (PCR)-based genotyping of *Pnky* and BAC*Pnky*—DNA from small tissue samples was prepared by boiling in 100μL of lysis buffer (0.2mM EDTA, 25mM NaOH) for 1 hr, followed by quenching in 100μL of neutralization buffer (40mM Tris HCl pH 7.5). Genotyping was performed using GoTaq (Promega, M3001) and the following reaction components, for a final volume of 12μL per reaction: 7.76μL of H_2O, 2.4μL of 5x buffer, 0.36μL of 50mM $MgCl_2$, 0.24μL of 10mM DNTPs, 0.12μL of primer mix (with each primer at 10μM), 0.12μL of GoTaq, 1μL of sample DNA. Reactions were incubated on a thermocycler as follows: 94°C for 2 min; 35 cycles of 94°C for 30 seconds (s), 60°C for 30 s, and 72°C for 1 min; 72°C for 5 min; 4°C hold. Reaction products were separated on a 2% agarose gel with ethidium bromide. The following primers were used (all listed 5’ to 3’):

Primers for *Pnky*^{F}, *Pnky*$^{+}$ and *Pnky*^{null} alleles: *Pnky* GT F: TAAGCTCAAACTCCGGTCCCGGGA

Pnky GT R1: TCAGGGACAAAGAACCAAAACGAGC

Pnky GT R2: AATGCTCCCTCTGAGCCTCAATT

Reaction products: 120bp (*Pnky*^{null}), 221bp (*Pnky*$^{+}$), and 348 (*Pnky*^{F}). Since BAC*Pnky* contains unaltered *Pnky*, this will produce the 221bp product, even in the absence of endogenous *Pnky* (see next section: Quantitative PCR (qPCR)-based genotyping for BAC*Pnky*).

Primers for BAC*Pnky*: BAC GT F: CACCTGCTACCTGATATAGGA

BAC GT R: CAGCAGTAATAGCAAGAGCA

Reaction product: 416bp (contains BAC*Pnky*). No amplification in the absence of BAC*Pnky*.

Quantitative PCR (qPCR)-based genotyping for BAC^{Pnky}—Because BAC^{Pnky} contains unmodified *Pnky*, it is indistinguishable from *Pnky*$^{+}$ in standard PCR-based genotyping. Therefore, certain genetic crosses required the use of qPCR to determine the endogenous *Pnky* alleles. This was done using 25ng of sample DNA (prepared as described above), along with 4μL SYBR green (Roche) and 2μL of primer mix (with each primer at 5μM) per 8μL qPCR reaction. Reactions were amplified on a LightCycler 480 II (Roche) using standard conditions. To quantify the number of copies of particular endogenous *Pnky* alleles, the $\Delta\Delta C_t$ method was used: a control genomic region was used to normalize for DNA content per reaction, and multiple samples with known endogenous *Pnky* alleles were used to compare to unknown samples.

Primers for control genomic region: Ctrl qPCR GT F: TGGTCGTTCTACAGGCCTTC

Ctrl qPCR GT R: GGACCGGTGACAGAGAACTG

Primers for *Pnky*^{null} allele: *Pnky* qPCR GT F: AGTTGGTCGTCCGCGTACGGTAC

Pnky^{null} qPCR GT R (same as *Pnky* GT R1): TCAGGGACAAAGAACCAAAACGAGC

Product: 97bp from *Pnky*^{null} allele. No amplification from other *Pnky* alleles or BAC^{Pnky}.

Primers for *Pnky*^{F} allele: *Pnky* qPCR GT F: AGTTGGTCGTCCGCGTACGGTAC

Pnky^{F} qPCR GT R: CCGGATCTTTCCTTTACCCGCAATAAC

Product: 228bp from *Pnky*^{F} allele. No amplification from other *Pnky* alleles or BAC^{Pnky}.

BrdU administration—Mice were administered 5-bromo-2'-deoxyuridine (BrdU, Millipore Sigma) reconstituted in sterile PBS through intraperitoneal injection, at a dose of 50mg BrdU per kg of mouse weight.

Tissue/cell preparation—Cultured cells were fixed in 4% paraformaldehyde (PFA, Millipore Sigma 158127) for 30 min at RT. Embryonic specimens up to E13.5 were fixed in 4% PFA as whole heads, up to overnight (O/N) at 4°C. For E15.5 samples, brains were dissected out of the skull prior to fixation in 4% PFA, up to O/N at 4°C. Transcardiac perfusion was performed on postnatal animals with phosphate buffered saline (PBS) followed by 4% PFA. The brains were then dissected out of the skull and additionally fixed in 4% PFA O/N at 4°C. All brain specimens were rinsed in PBS and then cryoprotected with 30% sucrose in PBS. Cryoprotected brains were then equilibrated in a 1:1 mixture of 30% sucrose and Tissue-Tek Optimal Cutting Temperature (OCT) (Thermo Fisher Scientific) for 1 hour (hr) at 4°C, then frozen in a fresh batch of the same mixture using dry ice. Frozen brain blocks were equilibrated in the cryostat at −23°C for at least 3 hrs prior to sectioning. Coronal sections with a thickness of 12-14μm were collected on Superfrost Plus Microscope Slides (Thermo Fisher Scientific) and stored at −80°C. Prior to IHC, tissue slides were rinsed in PBS with rotation for 10 minutes (min) at room temperature (RT) to remove sucrose/OCT.

Immunohistochemistry (IHC) and immunocytochemistry (ICC)—IHC and ICC were performed using blocking buffer consisting of PBS with 1% BSA (Millipore Sigma), 0.3M glycine (Thermo Fisher Scientific), 0.3% TritonX100 (Millipore Sigma), and either 10% normal goat serum or 10% normal donkey serum (Jackson ImmunoResearch Laboratories) depending on the species of origin of the secondary antibodies to be used. IHC was performed on tissue sections and ICC was performed on cells as follows:

Blocking: incubated in blocking buffer for 1-2 hrs (IHC) or 1 hr (ICC) at RT.

Primary antibodies: incubated in primary antibodies diluted in blocking buffer O/N at 4°C (IHC) or 2 hrs at RT (ICC).

Wash 1: washed 3 times in PBS at RT for 10 (IHC) or 5 min (ICC).

Secondary antibodies: incubated in secondary antibodies (Alexa Fluor antibodies from Thermo Fisher Scientific, 1:500) and DAPI (Thermo Fisher Scientific, 1:1000) diluted in blocking buffer for 30 min at RT (both IHC and ICC).

Wash 2: same as wash 1 above. This completed ICC.

Mounting coverslips: for IHC, slides were mounted with coverslips using Aqua Poly/Mount (Polysciences).

Antigen Retrieval—For certain antibodies (see below), antigen retrieval was performed using 10mM sodium citrate (pH 6.0) prior to IHC. Slides were incubated horizontally with 500μL of sodium citrate on top of the tissue for 2-3 min at RT. This was replaced with fresh sodium citrate, and the slides were moved to a pre-heated vegetable steamer. After 15 min, the slides were removed from the steamer and allowed to cool for 2-3 min at RT. The sodium citrate was then dumped off of the tissue and the slides were rinsed in PBS.

Primary antibodies for IHC/ICC—Please see Key Resources Table for antibody specifications. Antibodies were used as follows: **Tuj1**: diluted 1:1000 for ICC. **POU3F2**: diluted 1:250 for IHC (performed antigen retrieval for tissue of all ages). **CTIP2**: diluted 1:500 for IHC (performed antigen retrieval for postnatal tissue). **pH3**: diluted 1:400 for IHC. **pVim**: diluted 1:500 for IHC. **CUX1**: diluted 1:500 for IHC (performed antigen retrieval for postnatal tissue). **BrdU**: diluted 1:200 for IHC (performed antigen retrieval for tissue of all ages). **tdTomato** (Takara or Sicgen): diluted 1:500 for IHC or ICC (does not work after antigen retrieval, see below).

IHC for tdTomato in combination with antigen retrieval: IHC for tdTomato was performed as described above, then the tissue was re-fixed with 4% PFA for 45 minutes at RT. Slides were rinsed in PBS, then antigen retrieval was performed followed by IHC for the other antigens as described above.

***In Situ* Hybridization (ISH)—**ISH was performed on tissue sections (prepared as described above) using the RNAscope 2.5 HD Assay — BROWN. Probes targeting the mouse *Pnky* transcript were used (RNAscope Probe-Mm-Pnky).

Sample Preparation: Followed the Sample Preparation Technical Note for Fixed Frozen Tissue with the following modifications:

1. Before starting the protocol, let slides dry and then drew a barrier around tissue sections using ImmEdge Hydrophobic Barrier PAP Pen (Vector Laboratories). Let barrier dry, then rinsed tissue in PBS for 10 min at RT with rotation to remove sucrose/OCT. Post-fixed with 4% PFA for 20 min at RT, then rinsed in PBS for 5 min at RT. Started at Part 2: Tissue Pretreatment section of the Technical Note.
2. Instead of submerging slides in boiling Target Retrieval solution, added pre-heated Target Retrieval solution on top of horizontal slides and incubated in pre-heated vegetable steamer.
3. Used Protease III instead of Protease Plus. Incubated for 10 min at RT.

ISH: Followed the standard RNAscope 2.5 Assay protocol except for the following modifications:

1. Hybridized probes for 3 hrs.
2. Hybridized AMP 5 for 90 min.
3. Incubated in DAB for 1 hr.
4. For all wash steps, incubated for 2 min with gentle rotation instead of agitating (to preserve tissue integrity).

Microscopy and image analysis—Samples were imaged using Leica TCS SP5 X confocal, Leica DMi8, Leica DMI4000 B, and Keyence BZ-X710 inverted microscopes. For tissue samples that had received *in utero* injection of Ad:Cre, the contralateral hemisphere was analyzed whenever possible. For all other tissue samples, both hemispheres were analyzed from 2-4 non-adjacent regions. All image analysis and quantification was performed using Fiji (Schindelin et al., 2012). To quantify Tuj1+ area (Fig. 4H-I), the “threshold” and “measure” functions of Fiji were used.

RNA isolation—Total RNA was isolated from tissue and cultured cells using TRIzol (Thermo Fisher Scientific) and purified using Direct-zol RNA Purification Kits (Zymo Research). DNAse digestion was performed as suggested.

Quantitative reverse transcription PCR (qRT-PCR)—cDNA synthesis was performed using the Transcriptor First Strand cDNA synthesis kit (Roche). qRT-PCR was performed using SYBR green (Roche) on a LightCycler 480 II (Roche). Relative gene expression was calculated using the $\Delta\Delta C_t$ method, using *Rplp0* as a housekeeping gene for differential gene expression analyses. All qRT-PCR assays were performed using technical triplicate wells. See Key Resources Table for primer sequences.

RNA-seq library preparation—Prior to library preparation, RNA integrity was assessed using TapeStation 4200 (Agilent). Strand-specific poly(A) selected cDNA libraries were

generated using TruSeq Stranded mRNA kit (Illumina). Paired-end, 150bp sequencing of libraries was performed on a HiSeq 4000 (Illumina) by Novogene.

RNA Immunoprecipitation (RIP)—RIP using an antibody against PTBP1 (ThermoFisher) was performed as described previously (Ramos et al., 2015; Rinn et al., 2007) from cNSC cultures in 4 technical replicates from 2 separate experiments. The immunoprecipitated RNA was quantified by qRT-PCR using the percent input method. For each replicate, data were normalized to *β-actin* levels. *U1* was used as a negative control.

Cre-expressing adenovirus (Ad:Cre)—Ad:Cre (Merkle et al., 2007) was produced using 293A cells (Thermo Fisher Scientific, catalog number R70507). Concentrated adenovirus was prepared using the Fast Trap Adenovirus Purification and Concentration Kit (Millipore Sigma, catalog number FTAV00003).

***In utero* injections—**Injections were performed on timed-pregnant mice as previously described (Wang and Mei, 2013), except as follows: manual pipettes were used instead of mouth pipettes, and protocol sections 3.7-3.8 (delivery of electric pulses for electroporation) were skipped. Ad:Cre virus was mixed 1:1 with Trypan Blue to enable visualization of the injected solution. ~ 1μL of this mixture was injected into one of the lateral ventricles of E13.5 embryos. All protocols and procedures followed the guidelines of the Laboratory Animal Resource Center at the University of California, San Francisco and were conducted with IACUC approval.

Figure preparation—Figures were prepared using Photoshop and Illustrator (Adobe) and Prism (GraphPad).

QUANTIFICATION AND STATISTICAL ANALYSIS

All *in vivo* quantifications were normalized to littermate controls. For *in vivo* BAC rescue experiments, there was a low probability of obtaining all of the relevant experimental genotypes ($Pnky^{+/+}$, $Pnky^{null/null}$, and $Pnky^{null/null}$;BAC^{Pnky}) within the same litter. Therefore, we used one set of crosses to analyze $Pnky^{+/+}$ and $Pnky^{null/null}$ littermates as one group, and another set of crosses to analyze $Pnky^{null/null}$ and $Pnky^{null/null}$;BAC^{Pnky} littermates as a separate group. To compare phenotypes between these two groups, we normalized results to the genotype common to both ($Pnky^{null/null}$), as shown in (Fig. S4D).

For ICC quantification, technical triplicate wells of each genotype and treatment combination were analyzed. All cultures were normalized to their own treatment control.

The statistical details of each experiment can be found in the relevant figure legends, with additional details for RNA-seq experiments described below.

RNA-seq analysis of $Emx1^{Cre}$ experiments (Fig. S1 and Table S1): Reads were aligned to the mouse genome mm10 using Hisat2 v2.1.0 (Kim et al., 2015). At least 77 million mapped reads were obtained per sample. Differential gene expression was analyzed by DESeq2 (Love et al., 2014) and correction for multiple hypothesis testing was performed using the R package fdrtool (Strimmer, 2008). Transcription factor motif enrichment

analysis was performed on differentially-expressed gene sets using the Homer findMotifs.pl command (Heinz et al., 2010) with default settings, using all genes detected by RNA-seq as the background list.

Analysis of alternative splicing (including alternative exons, micro-exons, 3' and 5' splice sites, and retained introns) was performed using VAST-TOOLS v.1.0 (Braunschweig et al., 2014; Irimia et al., 2014). To determine if events were differentially spliced between the cortical tissues of *Pnky*-cKO and control mice, lowly-expressed transcripts (cRPKM < 3) and all events with low inclusion (PSI < 5%) were removed. The VAST-TOOLS diff module (Han et al., 2017) was used to both calculate the difference in percent spliced in (dPSI) between conditions and to identify statistically significant differences in splicing for all events with at least 10 reads support. All reported events were found to have significant dPSI: the probability of an event having |dPSI| of at least 5% is greater than 95%. Highly supported events have more than 10 reads mapping to the event in at least 50% of the profiled samples.

RNA-seq analysis of cNSC experiments (Fig. 4 and S4, and Table S2): Reads were pseudo-aligned to the Gencode M18 GRCm38.p6 transcriptome with Kallisto v0.43.1 (Bray et al., 2016). Differential expression analysis was performed using DESeq2 (Love et al., 2014), using the model (~ grp + grp:ind.n + grp:cnd) where grp = genotype, ind.n = individual biological replicate, and cnd = condition (untreated or +Ad:Cre) to identify genotype-specific effects of Ad:Cre. Correction for multiple hypothesis testing was performed using the R package fdrtool (Strimmer, 2008). As described above, transcription factor motif enrichment analysis was performed on differentially-expressed gene sets using the Homer findMotifs.pl command (Heinz et al., 2010) with default settings, using all genes detected by RNA-seq as the background list.

For splicing analysis, the data were aligned to the mouse genome by vast-tools (Braunschweig et al., 2014; Irimia et al., 2014)' with default options using *–mm10*. Analysis included all events that had at least 10 samples with 95% > PSI > 5% and for which vast-tools identified coverage as 'OK' or 'SOK' in at least 50% of samples. The VAST-TOOLS diff module (Han et al., 2017) was used to identify significantly differentially-spliced events, which required a minimum of 15 reads (-e 15) and called events significantly different between conditions only if |dPSI| > 0.05. A splicing event was deemed to be 'rescued' by BAC^{Pnky} if |dPSI| between *Pnky*$^{F/F}$;BAC^{Pnky} untreated and +Ad:Cre samples was < 0.05, |dPSI| between in *Pnky*$^{F/F}$ untreated and +Ad:Cre samples was significant, and if the rescue caused a shift away from *Pnky*-cKO conditions by at least |dPSI| > 0.05. For *Ptbp1*-KD comparison, we re-analyzed the data from previous studies in mouse N2a cells (Raj et al., 2014) and in V-SVZ NSCs (Ramos et al., 2015). From these two studies, we generated lists of events which were significantly affected by Ptbp1-KD at a |dPSI| > 0.05 cut-off. We compared these events (N=230 overlapping events in 227 genes) to those we found to be regulated by Pnky (N=220 events in 182 genes).

DATA AND SOFTWARE AVAILABILITY

The RNA-seq datasets generated during this study are available in the public repository GEO, available at https://www.ncbi.nlm.nih.gov/geo/. Data are listed with the accession number GSE127987.

Supplementary Material

Refer to Web version on PubMed Central for supplementary material.

ACKNOWLEDGEMENT

We thank the lab of Dr. Georgia Panagiotakos, and in particular Arpana Arjun for sharing expertise with *in utero* injections. We are grateful to the lab of Dr. Arturo Alvarez-Buylla for providing Ad:Cre virus, and to lab members Cristina Guinto for technical expertise and Dr. Kirsten Obernier for thoughtful discussions. We acknowledge Dr. Rebecca A. Ihrie for helpful advice on generating highly-concentrated adenovirus. We appreciate Dr. Aaron Diaz for feedback regarding statistical analyses. Finally, we thank Charlotte Bravo for her technical assistance. This work was supported by National Institutes of Health (NIH) 1F31NS098562-02 to R.E.A. and NIH 5R01NS091544–02, NIH 1R21NS101395–01, and Veterans Affairs 5I01 BX000252–07 to D.A.L.

REFERENCES

Anderson KM, Anderson DM, McAnally JR, Shelton JM, Bassel-Duby R, and Olson EN (2016). Transcription of the non-coding RNA upperhand controls Hand2 expression and heart development. Nature 539, 433–436. [PubMed: 27783597]

Aprea J, Prenninger S, Dori M, Ghosh T, Monasor LS, Wessendorf E, Zocher S, Massalini S, Alexopoulou D, Lesche M, et al. (2013). Transcriptome sequencing during mouse brain development identifies long non-coding RNAs functionally involved in neurogenic commitment. EMBO J. 32, 3145–3160. [PubMed: 24240175]

Arnold SJ, Huang G-J, Cheung AFP, Era T, Nishikawa S-I, Bikoff EK, Molnár Z, Robertson EJ, and Groszer M (2008). The T-box transcription factor Eomes/Tbr2 regulates neurogenesis in the cortical subventricular zone. Genes Dev. 22, 2479–2484. [PubMed: 18794345]

Barry G, Briggs JA, Vanichkina DP, Poth EM, Beveridge NJ, Ratnu VS, Nayler SP, Nones K, Hu J, Bredy TW, et al. (2014). The long non-coding RNA Gomafu is acutely regulated in response to neuronal activation and involved in schizophrenia-associated alternative splicing. Mol. Psychiatry 19, 486–494. [PubMed: 23628989]

Bassett AR, Akhtar A, Barlow DP, Bird AP, Brockdorff N, Duboule D, Ephrussi A, Ferguson-Smith AC, Gingeras TR, Haerty W, et al. (2014). Considerations when investigating lncRNA function in vivo. Elife 3, e03058. [PubMed: 25124674]

Bond AM, Vangompel MJW, Sametsky E. a, Clark MF, Savage JC, Disterhoft JF, and Kohtz JD (2009). Balanced gene regulation by an embryonic brain ncRNA is critical for adult hippocampal GABA circuitry. Nat. Neurosci 12, 1020–1027. [PubMed: 19620975]

Braunschweig U, Barbosa-Morais NL, Pan Q, Nachman EN, Alipanahi B, Gonatopoulos-Pournatzis T, Frey B, Irimia M, and Blencowe BJ (2014). Widespread intron retention in mammals functionally tunes transcriptomes. Genome Res. 24, 1774–1786. [PubMed: 25258385]

Bray NL, Pimentel H, Melsted P, and Pachter L (2016). Near-optimal probabilistic RNA-seq quantification. Nat. Biotechnol 34, 525–527. [PubMed: 27043002]

Briata P, Di Blas E, Gulisano M, Mallamaci A, lannone R, Boncinelli E, and Corte G (1996). EMX1 homeoprotein is expressed in cell nuclei of the developing cerebral cortex and in the axons of the olfactory sensory neurons. Mech. Dev 57, 169–180. [PubMed: 8843394]

Briggs JA, Wolvetang EJ, Mattick JS, Rinn JL, and Barry G (2015). Mechanisms of Long Non-coding RNAs in Mammalian Nervous System Development, Plasticity, Disease, and Evolution. Neuron 88, 861–877. [PubMed: 26637795]

Cajigas I, Chakraborty A, Swyter KR, Luo H, Bastidas M, Nigro M, Morris ER, Chen S, VanGompel MJW, Leib D, et al. (2018). The Evf2 Ultraconserved Enhancer lncRNA Functionally and

Spatially Organizes Megabase Distant Genes in the Developing Forebrain. Mol. Cell 71, 956–972.e9. [PubMed: 30146317]

Currle DS, Hu JS, Kolski-Andreaco A, and Monuki ES (2007). Culture of Mouse Neural Stem Cell Precursors. J. Vis. Exp e152–e152.

Djebali S, Davis CA, Merkel A, Dobin A, Lassmann T, Mortazavi A, Tanzer A, Lagarde J, Lin W, Schlesinger F, et al. (2012). Landscape of transcription in human cells. Nature 489, 101–108. [PubMed: 22955620]

Dominguez MH, Ayoub AE, and Rakic P (2013). POU-III transcription factors (Brn1, Brn2, and Oct6) influence neurogenesis, molecular identity, and migratory destination of upper-layer cells of the cerebral cortex. Cereb. Cortex 23, 2632–2643.

Durak O, de Anda FC, Singh KK, Leussis MP, Petryshen TL, Sklar P, and Tsai L-H (2015). Ankyrin-G regulates neurogenesis and Wnt signaling by altering the subcellular localization of β-catenin. Mol. Psychiatry 20, 388–397. [PubMed: 24821222]

Engreitz JM, Haines JE, Perez EM, Munson G, Chen J, Kane M, McDonel PE, Guttman M, and Lander ES (2016). Local regulation of gene expression by lncRNA promoters, transcription and splicing. Nature 539, 452–455. [PubMed: 27783602]

Gorski J. a, Talley T, Qiu M, Puelles L, Rubenstein JLR, and Jones KR (2002). Cortical excitatory neurons and glia, but not GABAergic neurons, are produced in the Emx1-expressing lineage. J. Neurosci 22, 6309–6314. [PubMed: 12151506]

Han H, Braunschweig U, Gonatopoulos-Pournatzis T, Weatheritt RJ, Hirsch CL, Ha KCH, Radovani E, Nabeel-Shah S, Sterne-Weiler T, Wang J, et al. (2017). Multilayered Control of Alternative Splicing Regulatory Networks by Transcription Factors. Mol. Cell 65, 539–553.e7. [PubMed: 28157508]

Heinz S, Benner C, Spann N, Bertolino E, Lin YC, Laslo P, Cheng JX, Murre C, Singh H, and Glass CK (2010). Simple combinations of lineage-determining transcription factors prime cis-regulatory elements required for macrophage and B cell identities. Mol. Cell 38, 576–589. [PubMed: 20513432]

Hudlebusch HR, Skotte J, Santoni-Rugiu E, Zimling ZG, Lees MJ, Simon R, Sauter G Rota R, De Ioris MA, Quarto M, et al. (2011). MMSET Is Highly Expressed and Associated with Aggressiveness in Neuroblastoma. Cancer Res. 71, 4226–4235. [PubMed: 21527557]

Imayoshi I, and Kageyama R (2014). Oscillatory control of bHLH factors in neural progenitors. Trends Neurosci. 37, 531–538. [PubMed: 25149265]

Irimia M, Weatheritt RJ, Ellis JD, Parikshak NN, Gonatopoulos-Pournatzis T, Babor M, Quesnel-Vallières M, Tapial J, Raj B, O'Hanlon D, et al. (2014). A Highly Conserved Program of Neuronal Microexons Is Misregulated in Autistic Brains. Cell 159, 1511–1523. [PubMed: 25525873]

Kaczmarek JC, Kowalski PS, and Anderson DG (2017). Advances in the delivery of RNA therapeutics: from concept to clinical reality. Genome Med. 9, 60. [PubMed: 28655327]

Kim D, Langmead B, and Salzberg SL (2015). HISAT: a fast spliced aligner with low memory requirements. Nat. Methods 12, 357–360. [PubMed: 25751142]

Kopp F, and Mendell JT (2018). Functional Classification and Experimental Dissection of Long Noncoding RNAs. Cell 172, 393–407. [PubMed: 29373828]

Lakso M, Pichel JG, Gorman JR, Sauer B, Okamoto Y, Lee E, Alt FW, and Westphal H (1996). Efficient in vivo manipulation of mouse genomic sequences at the zygote stage. Proc. Natl. Acad. Sci. U. S. A 93, 5860–5865. [PubMed: 8650183]

Lenstra TL, Rodriguez J, Chen H, and Larson DR (2016). Transcription Dynamics in Living Cells. Annu. Rev. Biophys 45, 25–47. [PubMed: 27145880]

Liu SJ, and Lim DA (2018). Modulating the expression of long non-coding RNAs for functional studies. EMBO Rep. 19, e46955. [PubMed: 30467236]

Liu SJ, Horlbeck MA, Cho SW, Birk HS, Malatesta M, He D, Attenello FJ, Villalta JE, Cho MY, Chen Y, et al. (2017). CRISPRi-based genome-scale identification of functional long noncoding RNA loci in human cells. Science 355, eaah7111.

Lodato S, and Arlotta P (2015). Generating Neuronal Diversity in the Mammalian Cerebral Cortex. Annu. Rev. Cell Dev. Biol 31, 699–720. [PubMed: 26359774]

Lodato S, Rouaux C, Quast KB, Jantrachotechatchawan C, Studer M, Hensch TK, and Arlotta P (2011). Excitatory Projection Neuron Subtypes Control the Distribution of Local Inhibitory Interneurons in the Cerebral Cortex. Neuron 69, 763–779. [PubMed: 21338885]

Love MI, Huber W, and Anders S (2014). Moderated estimation of fold change and dispersion for RNA-seq data with DESeq2. Genome Biol. 15, 550. [PubMed: 25516281]

Luo S, Lu JY, Liu L, Yin Y, Chen C, Han X, Wu B, Xu R, Liu W, Yan P, et al. (2016). Divergent lncRNAs Regulate Gene Expression and Lineage Differentiation in Pluripotent Cells. Cell Stem Cell 18, 637–652. [PubMed: 26996597]

Madisen L, Zwingman TA, Sunkin SM, Oh SW, Zariwala HA, Gu H, Ng LL, Palmiter RD, Hawrylycz MJ, Jones AR, et al. (2010). A robust and high-throughput Cre reporting and characterization system for the whole mouse brain. Nat. Neurosci 13, 133–140. [PubMed: 20023653]

Meng L, Ward AJ, Chun S, Bennett CF, Beaudet AL, and Rigo F (2015). Towards a therapy for Angelman syndrome by targeting a long non-coding RNA. Nature 518, 409–412. [PubMed: 25470045]

Merkle FT, Mirzadeh Z, and Alvarez-Buylla A (2007). Mosaic organization of neural stem cells in the adult brain. Science 317, 381–384. [PubMed: 17615304]

Mesman S, and Smidt MP (2017). Tcf12 Is Involved in Early Cell-Fate Determination and Subset Specification of Midbrain Dopamine Neurons. Front. Mol. Neurosci 10, 353. [PubMed: 29163030]

Molyneaux BJ, Arlotta P, Hirata T, Hibi M, and Macklis JD (2005). Fezl Is Required for the Birth and Specification of Corticospinal Motor Neurons. Neuron 47, 817–831. [PubMed: 16157277]

Molyneaux BJ, Arlotta P, Menezes JRL, and Macklis JD (2007). Neuronal subtype specification in the cerebral cortex. Nat. Rev. Neurosci 8, 427–437. [PubMed: 17514196]

Nakagawa S (2016). Lessons from reverse-genetic studies of lncRNAs. Biochim. Biophys. Acta - Gene Regul. Mech 1859, 177–183.

Ørom UA, Derrien T, Beringer M, Gumireddy K, Gardini A, Bussotti G, Lai F, Zytnicki M, Notredame C, Huang Q, et al. (2010). Long noncoding RNAs with enhancer-like function in human cells. Cell 143, 46–58. [PubMed: 20887892]

Pavlaki I, Alammari F, Sun B, Clark N, Sirey T, Lee S, Woodcock DJ, Ponting CP, Szele FG, and Vance KW (2018). The long non-coding RNA *Paupar* promotes KAP1-dependent chromatin changes and regulates olfactory bulb neurogenesis. EMBO J. 37, e98219. [PubMed: 29661885]

Perez-Garcia CG (2015). ErbB4 in Laminated Brain Structures: A Neurodevelopmental Approach to Schizophrenia. Front. Cell. Neurosci 9, 472.

Peukert D, Weber S, Lumsden A, and Scholpp S (2011). Lhx2 and Lhx9 Determine Neuronal Differentiation and Compartition in the Caudal Forebrain by Regulating Wnt Signaling. PLoS Biol. 9, e1001218. [PubMed: 22180728]

Raj B, Irimia M, Braunschweig U, Sterne-Weiler T, O'Hanlon D, Lin Z-Y, Chen GI, Easton LE, Ule J, Gingras A-C, et al. (2014). A Global Regulatory Mechanism for Activating an Exon Network Required for Neurogenesis. Mol. Cell 56, 90–103. [PubMed: 25219497]

Ramos AD, Andersen RE, Liu SJ, Nowakowski TJ, Hong SJ, Gertz CC, Salinas RD, Zarabi H, Kriegstein AR, and Lim DA (2015). The long noncoding RNA Pnky regulates neuronal differentiation of embryonic and postnatal neural stem cells. Cell Stem Cell 16, 439–447. [PubMed: 25800779]

Rapicavoli NA, Poth EM, Zhu H, and Blackshaw S (2011). The long noncoding RNA Six3OS acts in trans to regulate retinal development by modulating Six3 activity. Neural Dev. 6, 32. [PubMed: 21936910]

Rinn JL, Kertesz M, Wang JK, Squazzo SL, Xu X, Brugmann S. a., Goodnough LH, Helms J. a., Farnham PJ, Segal E, et al. (2007). Functional Demarcation of Active and Silent Chromatin Domains in Human HOX Loci by Noncoding RNAs. Cell 129, 1311–1323. [PubMed: 17604720]

Rubenstein JLR (2011). Annual Research Review: Development of the cerebral cortex: implications for neurodevelopmental disorders. J. Child Psychol. Psychiatry. 52, 339–355. [PubMed: 20735793]

Ruzankina Y, Pinzon-Guzman C, Asare A, Ong T, Pontano L, Cotsarelis G, Zediak VP, Velez M, Bhandoola A, and Brown EJ (2007). Deletion of the Developmentally Essential Gene ATR in

Adult Mice Leads to Age-Related Phenotypes and Stem Cell Loss. Cell Stem Cell 1, 113–126. [PubMed: 18371340]

Sauvageau M, Goff LA, Lodato S, Bonev B, Groff AF, Gerhardinger C, Sanchez-Gomez DB, Hacisuleyman E, Li E, Spence M, et al. (2013). Multiple knockout mouse models reveal lincRNAs are required for life and brain development. Elife 2, e01749. [PubMed: 24381249]

Schindelin J, Arganda-Carreras I, Frise E, Kaynig V, Longair M, Pietzsch T, Preibisch S, Rueden C, Saalfeld S, Schmid B, et al. (2012). Fiji: an open-source platform for biological-image analysis. Nat. Methods 9, 676–682. [PubMed: 22743772]

Silva CG, Peyre E, Adhikari MH, Tielens S, Tanco S, Van Damme P, Magno L, Krusy N, Agirman G, Magiera MM, et al. (2018). Cell-Intrinsic Control of Interneuron Migration Drives Cortical Morphogenesis. Cell 172, 1063–1078.e19. [PubMed: 29474907]

Simeone A, Acampora D, Gulisano M, Stornaiuolo A, and Boncinelli E (1992). Nested expression domains of four homeobox genes in developing rostral brain. Nature 358, 687–690. [PubMed: 1353865]

Spadaro PA, Flavell CR, Widagdo J, Ratnu VS, Troup M, Ragan C, Mattick JS, and Bredy TW (2015). Long noncoding RNA-directed epigenetic regulation of gene expression is associated with anxiety-like behavior in mice. Biol. Psychiatry 78, 848–859. [PubMed: 25792222]

Strimmer K (2008). fdrtool: a versatile R package for estimating local and tail area-based false discovery rates. Bioinformatics 24, 1461–1462. [PubMed: 18441000]

Vance KW, Sansom SN, Lee S, Chalei V, Kong L, Cooper SE, Oliver PL, and Ponting CP (2014). The long non-coding RNA Paupar regulates the expression of both local and distal genes. EMBO J. 33, 296–311. [PubMed: 24488179]

Wagschal A, Rousset E, Basavarajaiah P, Contreras X, Harwig A, Laurent-Chabalier S, Nakamura M, Chen X, Zhang K, Meziane O, et al. (2012). Microprocessor, Setx, Xrn2, and Rrp6 co-operate to induce premature termination of transcription by RnAPII. Cell 150, 1147–1157. [PubMed: 22980978]

Wang C, and Mei L (2013). In Utero Electroporation in Mice. (Humana Press, Totowa, NJ), pp. 151–163.

Wang KC, Yang YW, Liu B, Sanyal A, Corces-Zimmerman R, Chen Y, Lajoie BR, Protacio A, Flynn RA, Gupta RA, et al. (2011). A long noncoding RNA maintains active chromatin to coordinate homeotic gene expression. Nature 472, 120–124. [PubMed: 21423168]

Warming S, Costantino N, Court DL, Jenkins NA, and Copeland NG (2005). Simple and highly efficient BAC recombineering using galK selection. Nucleic Acids Res. 33, e36. [PubMed: 15731329]

West S, Gromak N, and Proudfoot NJ (2004). Human 5’ → 3’ exonuclease Xrn2 promotes transcription termination at co-transcriptional cleavage sites. Nature 432, 522–525. [PubMed: 15565158]

Zhang S, Li J, Lea R, Vleminckx K, and Amaya E (2014). Fezf2 promotes neuronal differentiation through localised activation of Wnt/β-catenin signalling during forebrain development. Development 141, 4794–4805. [PubMed: 25468942]

Zhang X, Chen MH, Wu X, Kodani A, Fan J, Doan R, Ozawa M, Ma J, Yoshida N, Reiter JF, et al. (2016). Cell-Type-Specific Alternative Splicing Governs Cell Fate in the Developing Cerebral Cortex. Cell 166, 1147–1162.e15. [PubMed: 27565344]

Highlights:

- *Pnky* is a long noncoding RNA (lncRNA) that regulates cortical development *in vivo*.
- *Pnky* acts cell-autonomously to affect neuron production in the developing cortex.
- Despite its divergent configuration with *Pou3f2, Pnky* does not regulate *Pou3f2*.
- BAC transgenic rescue demonstrates that *Pnky* functions in *trans*.

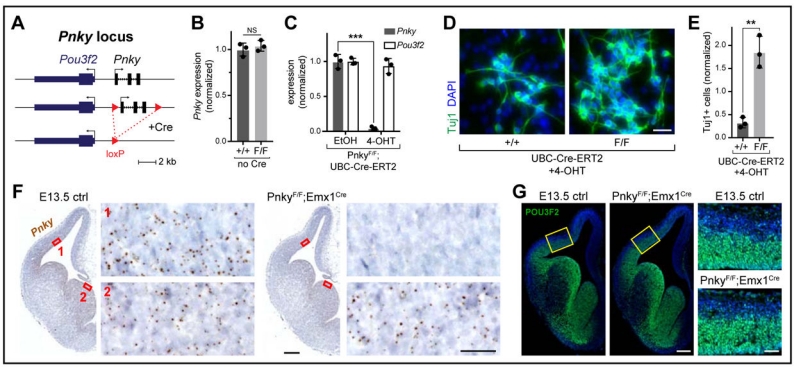

Figure 1: Generation of a conditional deletion allele for the lncRNA *Pnky*

Quantifications: mean +/− SD. NS = not significant, ** = $p < 0.01$, *** = $p < 0.001$, unpaired two-tailed t test. **A**, Schematic of *Pnky* locus and loxP site insertions. **B**, *Pnky* levels in V-SVZ cultures by qRT-PCR. Biological replicate littermates, normalized to *Pnky* $^{+/+}$ mean. **C**, *Pnky* and *Pou3f2* in ethanol (EtOH)- or 4-OHT-treated V-SVZ cultures by qRT-PCR. Technical replicates, normalized to EtOH-treated mean. **D**, Tuj1 ICC in d4 differentiated V-SVZ cultures. Scale bar = 25μm. **E**, Quantification of (D). Technical replicates with independent EtOH or 4-OHT treatment, normalized to EtOH-treated cultures for each genotype. **F**, ISH of *Pnky* (brown puncta) in coronal brain sections, with hematoxylin nuclear counterstain (blue). Red boxes = regions of pallium (1) and subpallium (2) enlarged in adjacent panels. Scale bars = 250μm (hemispheres) and 25μm (insets). **G**, POU3F2 IHC with DAPI nuclear stain (blue). Yellow boxes = regions of pallium enlarged in adjacent panels. Scale bars = 200μm (hemispheres) and 50μm (insets). See also Figure S1.

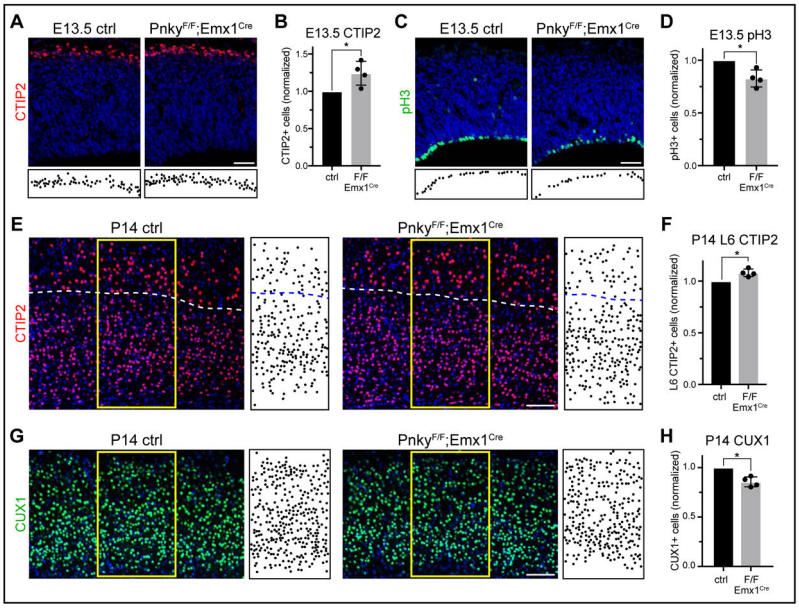

Figure 2: *Pnky* regulates cortical neurogenesis *in vivo*

Quantifications: mean +/− SD of biological replicates, normalized to littermate controls. * = $p < 0.05$, two-tailed ratio paired t test. **A**, CTIP2 IHC with DAPI (blue). Locations of CTIP2+ cells in CP depicted below. Scale bar = 50μm. **B**, Quantification of (A). **C**, pH3 IHC with DAPI (blue). Locations of pH3+ cells in VZ depicted below. Scale bar = 50μm. **D**, Quantification of (C). **E**, CTIP2 IHC in the deep layers of P14 cortex, with DAPI (blue). Dotted line = border between L5 and L6. Locations of CTIP2+ cells within yellow boxes depicted to the right. Scale bar = 100μm. **F**, Quantification of (E). **G**, CUX1 IHC in the upper layers of P14 cortex, with DAPI (blue). Locations of CUX1+ cells within yellow boxes depicted to the right. Scale bar = 100μm. **H**, Quantification of (G). See also Figure S2.

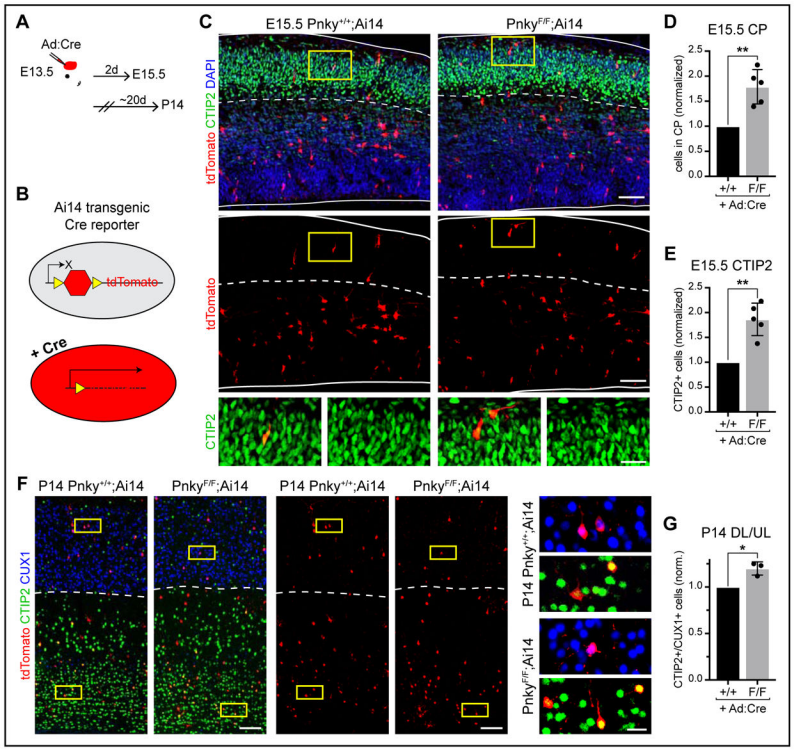

Figure 3: *Pnky* functions cell-autonomously in the developing cortex

Quantifications: mean +/− SD of biological replicates, normalized to littermate controls. * = $p < 0.05$, ** = $p < 0.01$, two-tailed ratio paired t test. **A**, Schematic of *in utero* Ad:Cre viral injections. **B**, Schematic of Ai14 transgenic Cre reporter. **C**, IHC of tdTomato and CTIP2 at E15.5. Arrowheads = double-positive cells within CP, demarcated by dotted line. Yellow boxes = regions enlarged below. Scale bars = 50μm and 20μm (insets). **D**, Quantification of proportion of tdTomato+ cells in the CP. **E**, Quantification of proportion of tdTomato+ cells located in CP and CTIP2+ (D). **F**, IHC for tdTomato, CTIP2, and CUX1 at P14. Dotted line = border between deep and upper cortical layers. Yellow boxes = regions enlarged in adjacent panels. Arrowheads = double-positive cells. Scale bars = 100μm and 20μm (insets). G, Quantification of ratio of CTIP2+ deep layer cells to CUX1+ upper layer cells within tdTomato+ population at P14. See also Figure S3.

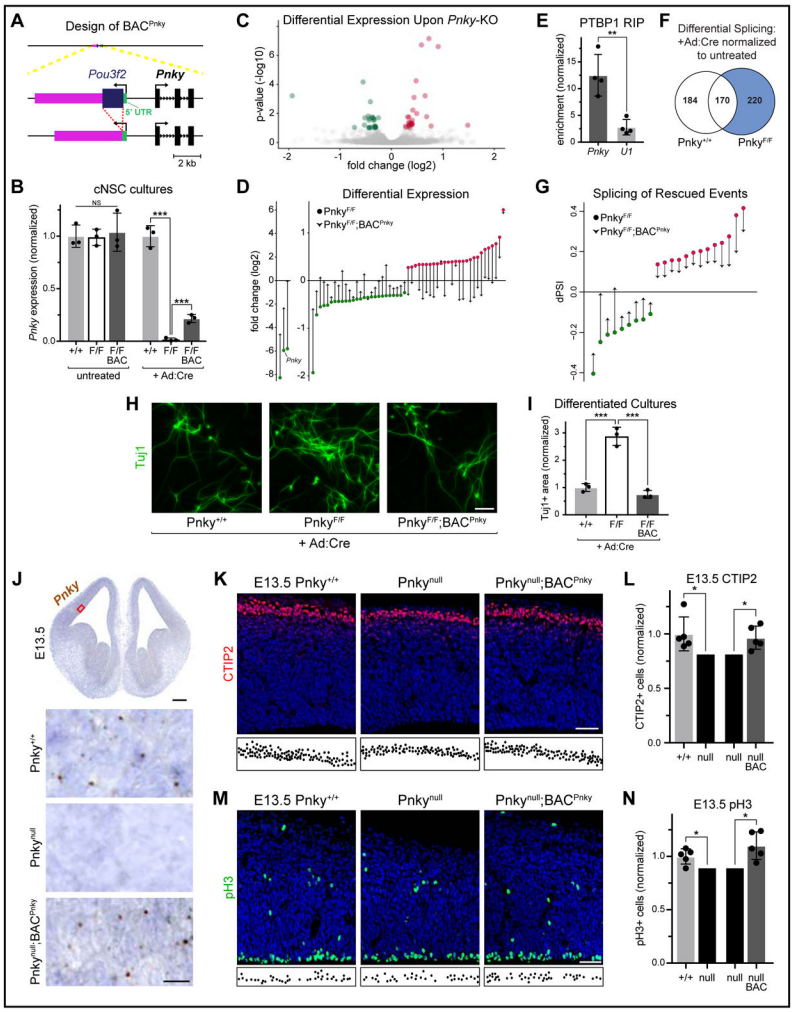

Figure 4: BAC transgenic expression of *Pnky* rescues loss of the endogenous lncRNA

Quantifications: mean +/− SD of separate biological replicates, except as indicated in (I). NS = not significant, * = $p < 0.05$, *** = $p < .001$. **A**, Schematic of BAC^{Pnky} transgene. **B**, *Pnky* expression in untreated or +Ad:Cre cNSC cultures by RNA-seq. Normalized to Pnky$^{+/+}$ mean for each treatment group. **C**, Volcano plot of differentially-expressed genes upon *Pnky*-cKO. Three genes with fold changes outside this range are not displayed here (see D). **D**, Log2 fold changes of all significantly differentially-expressed genes in Pnky$^{F/F}$ +Ad:Cre cultures (circles). Arrowheads = log2 fold changes for these genes in Pnky$^{F/F}$;BAC^{Pnky} +Ad:Cre cultures. **E**, Enrichment following RIP with PTBP1 antibodies from cNSC cultures. 4 technical replicates from 2 separate experiments, normalized to levels of *β-actin*. **F**, Alternatively-spliced events in cNSCs upon Ad:Cre treatment. Significant events in *Pnky*$^{F/F}$ +Ad:Cre samples that did not overlap with events in *Pnky*$^{+/+}$ +Ad:Cre samples were analyzed further. **G**, Log2 fold changes of rescued alternatively-spliced events. **H**, Tuj1 ICC in d7 differentiated cNSC cultures. Scale bar = 50μm. I, Quantification of Tuj1+ area from (H). Mean +/− SD from technical triplicates comprised of cells pooled from three biological replicates. Normalized to uninfected controls and to *Pnky*$^{+/+}$ +Ad:Cre values. Statistical analysis = one-way ANOVA with Turkey's multiple comparisons test. **J**, ISH of *Pnky*

(brown puncta) with hematoxylin counterstain (blue). Representative section with red box indicating approximate region of pallium enlarged below. Scale bars = 250μm and 25μm (insets). **K**, CTIP2 IHC with DAPI (blue). Locations of CTIP2+ cells in CP depicted below. Scale bar = 50μm. **L**, Quantification of (K), two-tailed ratio paired t test. **M**, pH3 IHC with DAPI (blue). Locations of pH3+ cells in VZ depicted below. Scale bar = 50μm. **N**, Quantification of (M), two-tailed ratio paired t test. See also Figure S4 and Table S2.

KEY RESOURCES TABLE

REAGENT or RESOURCE	SOURCE	IDENTIFIER
Antibodies		
Anti-Tubulin β3 (Tuj1)	Biolegend	Cat. # 801201
Anti-POU3F2	Cell Signaling Technology	Cat. # 12137
Anti-CTIP2	Abcam	Cat. # ab18465
Anti-phospho-histone H3 (pH3)	Millipore Sigma	Cat. # 06570
Anti-phosphorylated vimentin (pVim)	MBL	Cat. # D076-3
Anti-CUX1	Santa Cruz	Cat. # sc-13024
Anti-BrdU	Abcam	Cat. # ab6326
Anti-tdTomato	Takara	Cat. # 632496
Anti-tdTomato	Sicgen	Cat. # AB8181-200
Anti-PTBP1	ThermoFisher	Cat. # 32-4800
Bacterial and Virus Strains		
Ad:Cre	Alvarez-Buylla Lab	Merkle et al., 2007
Chemicals, Peptides, and Recombinant Proteins		
4-Hydroxytamoxifen (4-OHT)	Millipore Sigma	Cat. # H7904
5-Bromo-2′-deoxyuridine (BrdU)	Millipore Sigma	Cat. # B5002
Critical Commercial Assays		
RNAscope 2.5 HD Assay — BROWN	Advanced Cell Diagnostics	Cat. # 322300
RNAscope Probe-Mm-Pnky	Advanced Cell Diagnostics	Cat. # 405551
Deposited Data		
RNA-seq: *Emx1*-Cre cortex and cNSC cultures	This paper	GEO: GSE127987
Experimental Models: Organisms/Strains		
Mouse: wild-type: C57BL/6J	The Jackson Laboratory	MGI: 3028467
Mouse: UBC-Cre-ERT2: Ndor1$^{Tg(UBC-cre/ERT2)1Ejb}$	The Jackson Laboratory	Ruzankina et al., 2007
Mouse: *Emx1*^{Cre}: Emx1$^{tm1(cre)Krj}$	The Jackson Laboratory	Gorski et al., 2002
Mouse: Ai14: Gt(ROSA)26Sor$^{tm14(CAG-tdTomato)Hze}$	The Jackson Laboratory	Madisen et al., 2010
Mouse: E2a-Cre: Tg(EIIa-cre)C5379Lmgd	The Jackson Laboratory	Lakso et al., 1996
Mouse: *Pnky*^{F}	This paper	N/A
Mouse: *Pnky*^{null}	This paper	N/A
Mouse: BAC^{Pnky}	This paper	N/A
Oligonucleotides		
qPCR: *Rplp0* F: CCGATCTGCAGACACACACT	Ramos et al., 2013	N/A
qPCR: *Rplp0* R: ACCCTGAAGTGCTCGACATC	Ramos et al., 2013	N/A
qPCR: *Pnky* F: TCTCCTTTCTCCGCCAGTAA	Ramos et al., 2015	N/A
qPCR: *Pnky* R: CACCGCTTCTTGTCAGTTCA	Ramos et al., 2015	N/A
qPCR: *Pou3f2* F: ATGTGCAAGCTGAAGCCTTT	Bonvin et al., 2012	N/A

REAGENT or RESOURCE	SOURCE	IDENTIFIER
qPCR: *Pou3f2* R: CTCACCACCTCCTTCTCCAG	Bonvin et al., 2012	N/A
qPCR: *U1* F: ACGAAGGTGGTTTTCCCAG	Ramos et al., 2015	N/A
qPCR: *U1* R: GTCCCCCACTACCACAAA	Ramos et al., 2015	N/A
qPCR: *β-actin* F: CTAAGGCCAACCGTGAAAAG	Ramos et al., 2015	N/A
qPCR: *β-actin* R: ACCAGAGGCATACAGGGACA	Ramos et al., 2015	N/A
Recombinant DNA		
BAC containing the mouse *Pnky* locus	BACPAC Resources Center	Clone RP23-451I6
Software and Algorithms		
Hisat2 v2.1.0	Kim et al., 2015	https://ccb.jhu.edu/software/hisat2/index.shtml
DESeq2	Love et al., 2014	https://bioconductor.org/packages/release/bioc/html/DESeq2.html
fdrtool	Strimmer, 2008	https://CRAN.R-project.org/package=fdrtool
Homer findMotifs.pl	Heinz et al., 2010	http://homer.ucsd.edu/homer/motif/
VAST-TOOLS v.1.0; VAST-TOOLS diff module	Braunschweig et al., 2014; Irimia et al., 2014; Han et al., 2017	https://github.com/vastgroup/vast-tools
Kallisto v0.43.1	Bray et al., 2016	https://github.com/pachterlab/kallisto/releases
Fiji / ImageJ	Schindelin et al., 2012	https://fiji.sc
Prism 7	GraphPad Software	N/A
Adobe Photoshop	Adobe Systems Inc.	N/A
Adobe Illustrator	Adobe Systems Inc.	N/A